Short-time behavior of advecting-diffusing scalar fields in Stokes flows

M. Giona,* P. D. Anderson, and F. Garofalo†

Materials Technology, Eindhoven University of Technology, PO Box 513, 5600, MB Eindhoven, The Netherlands

(Received 14 August 2012; revised manuscript received 14 March 2013; published 17 June 2013)

This article addresses the short-term decay of advecting-diffusing scalar fields in Stokes flows. The analysis is developed in two main subparts. In the first part, we present an analytic approach for a class of simple flow systems expressed mathematically by the one-dimensional advection-diffusion equation $w(y)\partial_\xi\phi = \varepsilon\partial_y^2\phi + iV(y)\phi - \varepsilon'\phi$, where ξ is either time or axial coordinate and $iV(y)$ an imaginary potential. This class of systems encompasses both open- and closed-flow models and corresponds to the dynamics of a single Fourier mode in parallel flows. We derive an analytic expression for the short-time (short-length) decay of ϕ, and show that this decay is characterized by a universal behavior that depends solely on the singularity of the ratio of the transverse-to-axial velocity components $V_{\rm eff}(y) = V(y)/w(y)$, corresponding to the effective potential in the imaginary potential formulation. If $V_{\rm eff}(y)$ is smooth, then $||\phi||_{L^2}(\xi) = \exp(-\varepsilon'\xi - b\xi^3)$, where $b > 0$ is a constant. Conversely, if the effective potential is singular, then $||\phi||_{L^2}(\xi) = 1 - a\xi^\nu$ with $a > 0$. The exponent ν attains the value $\frac{5}{3}$ at the very early stages of the process, while for intermediate stages its value is $\frac{3}{5}$. By summing over all of the Fourier modes, a stretched exponential decay is obtained in the presence of nonimpulsive initial conditions, while impulsive conditions give rise to an early-stage power-law behavior. In the second part, we consider generic, chaotic, and nonchaotic autonomous Stokes flows, providing a kinematic interpretation of the results found in the first part. The kinematic approach grounded on the warped-time transformation complements the analytical theory developed in the first part.

DOI: 10.1103/PhysRevE.87.063011 PACS number(s): 47.15.−x, 83.50.Xa, 05.60.−k

I. INTRODUCTION

Mixing and transport in laminar flows admits several important implications in the processing of very viscous fluids for chemical and pharmaceutical applications [1,2] and in microfluidic technology [3,4]. The advection-diffusion equation is the fundamental Eulerian description of the interaction between a deterministic velocity field and stochastic fluctuations that give rise to a term proportional to the Laplacian of the scalar field [5]. For all the processes driven by stochastic fluctuations possessing uncorrelated increments (Wiener processes), the evolution of the probability density function satisfies a forward Fokker-Planck equation [5], which is essentially a particular form of an advection-diffusion equation. Consequently, the understanding of the general properties of the solutions of the advection-diffusion equation has important implications in many different fields of physical, biological, and social sciences: from soft-matter theory to stellar dynamics [6], from biological systems [7] to economical and financial models [8], from wave localization and propagation in layered and nonlayered random media, to impurity dynamics [9].

The research core in the field of advection-diffusion processes in laminar flows has been focused on the long-term asymptotic decay of scalar fields that is controlled by the eigenvalue and eigenvector structures of the advection-diffusion operator [10]. Several studies have also analyzed the early-stage and intermediate mixing dynamics. Meunier and Villermaux [11] analyzed the short-term decay of a concentration field in a vortex flow by focusing the attention on the probability density function of the advected scalar field. Ferreira de Sousa and Pereira [12] considered the early decay of a scalar field in a two-dimensional tripolar vortex for moderate values of the Schmidt number $Sc \in (0.1, 100)$, and consequently of the Péclet number. Intermediate power-law scalings of the norm of a concentration field have been also observed experimentally in chaotic flows in the presence of solid boundaries [13], and the effects of moving walls on the intermediate scalar decay have been addressed [14]. At these time ranges, the decay dynamics of a scalar field is a consequence of the linear superposition of many eigenmodes, and at the very early stages of all them, of the advection-diffusion operator, and it depends strongly on the initial condition since different initial conditions excite differently the eigenvalue and eigenmode spectra. Transient mixing effects in chaotic flows have been studied by Gleeson [15].

There is no general theory for the short-term properties of laminar flow systems. Consequently, it is interesting to investigate whether the short-term properties of advecting-diffusing scalars in Stokesian flows admit a universal behavior, at least for a class of initial conditions of physical interest and, if so, whether the early-stage dynamics could be predicted directly from the properties of the advection-diffusion operator.

As in the case of the analysis of the asymptotic behavior, a convenient strategy for addressing the early-stage properties could be the following: (i) first consider simple but nontrivial model flows for which a theoretical analysis can be performed analytically, and (ii) subsequently extend the results so obtained to generic Stokes flows. In this article, we follow this strategy in approaching the analysis of short-term properties. In the first part of this article (Secs. III and IV), we consider a class of model flows for which a fully analytical interpretation of the early-stage dynamics can be developed. This class is represented by (closed- or open-) flow systems

*Permanent address: Dipartimento di Ingegneria Chimica Materiali e Ambiente, La Sapienza Università di Roma, Via Eudossiana 18, 00184 Roma, Italy.

†Corresponding author: F.Garofalo@tue.nl

in which the dynamics of the Fourier coefficients of the scalar field decouples into a countable system of non-Hermitian Schrödinger-type equations in the presence of an imaginary potential.

Starting from the Schrödinger-type formulation, Giona *et al.* [16–18] have derived several spectral properties of advecting-diffusing systems, and the expression for the dominant exponent controlling generically the exponential decay of the norms of a scalar field as a function of the Péclet number [17]. The imaginary potential formulation is suitable for describing physically realizable magnetohydrodynamic micromixers [19], and for defining simple perturbation schemes in order to predict the spectral properties in the low and intermediate regions of Péclet number values [20]. As briefly outlined in Sec. II, the mathematical description of channel flows operating with time-pulsating inlets falls in the same class of problems.

We show that the short-term (short-time or short-length, depending on the operating conditions) behavior of simple mixing systems is characterized by the occurrence of a universal decay of the L^2-norm of scalar fields, the functional form of which depends on the singularity of the effective potential. The effective potential, introduced in Sec. III, is defined as the ratio of the transverse-to-axial velocity components.

Gathering together modal dynamics, and weighting it with respect to the Fourier coefficients associated with the initial condition, it is possible to obtain a global prediction of the norm decay for prototypical autonomous flows for nonimpulsive and impulsive initial conditions. A stretched exponential behavior is found for nonimpulsive conditions, while impulsive conditions give rise to a power-law decay.

The second part of this article (Secs. V and VI) presents the numerical results for the early-stage decay in prototypical Stokes flow (lid-driven cavity flow, ABC flow), and develops a simple kinematic interpretation of the results obtained. This kinematic interpretation is fully predictive and confirms the analytical results found in the first part of the article.

The article is organized as follows. Section II defines the concept of short-term, intermediate, and asymptotic dynamics in a simple physical way and introduces the basic model equation, the concept of imaginary potential, and the different flow phenomenologies this equation can describe. The Bohmian (modulus and phase) decomposition of the equation is also reviewed. Section III analyzes the short-term properties of the one-dimensional advection-diffusion equation in the presence of an imaginary potential in the two relevant cases, i.e., where the resulting effective potentials are a smooth versus singular function of the position. The imaginary potential formulation of the advection-diffusion equation describes the evolution of the decoupled Fourier modes of prototypical closed flow systems (such as the sine flow). As addressed in Sec. IV, it is possible to predict the early-stage decay in these systems for generic initial conditions (square summable, impulsive), gathering the contribution of each mode, leading to typical stretched-exponential or power-law scalings. Section V describes the numerical results obtained in physically realizable systems such as the lid-driven cavity flow, and model systems (the ABC flow) giving rise to partial Lagrangian chaos. A simple kinematic interpretation of the result found in Sec. V is developed in Sec. VI, providing a fully predictive model of the early-stage dynamics based on the warped-time transformation. The kinematic approach agrees qualitatively and quantitatively with the analysis developed in Sec. IV.

II. STATEMENT OF THE PROBLEM, MIXING REGIMES, AND PROTOTYPICAL FLOW SYSTEMS

Let us consider a scalar field $\phi(\mathbf{x},t)$ defined in a closed bounded mixing domain Ω (or on a boundaryless manifold), and let $\mathbf{v}(\mathbf{x},t)$ be a time-periodic deterministic incompressible velocity field. The evolution equation for $\phi(\mathbf{x},t)$ in the presence of diffusion reads in dimensionless form as

$$\partial_t \phi(\mathbf{x},t) = -\mathbf{v}(\mathbf{x},t)\cdot\nabla\phi(\mathbf{x},t) + \varepsilon\nabla^2\phi(\mathbf{x},t), \tag{1}$$

where $\varepsilon = \mathrm{Pe}^{-1}$ is the reciprocal of the Péclet number. Let $||\phi||_{L^2}(t)$ and $||\nabla\phi||_{L^2}(t)$ be the L^2 norms of ϕ and of its gradient

$$\begin{aligned} ||\phi||_{L^2}(t) &= \left[\int_\Omega \phi^2(\mathbf{x},t)\,d\mathbf{x}\right]^{1/2}, \\ ||\nabla\phi||_{L^2}(t) &= \left[\int_\Omega |\nabla\phi(\mathbf{x},t)|^2\,d\mathbf{x}\right]^{1/2}. \end{aligned} \tag{2}$$

If Ω is bounded, the velocity field on the boundary $\partial\Omega$ of Ω is at most tangential to the boundary, that is, $\mathbf{v}\cdot\mathbf{n}|_{\partial\Omega} = 0$ where $\mathbf{n}$ indicates the pointwise normal vector at $\partial\Omega$, and Eq. (1) is equipped with homogeneous Neumann conditions $\partial\phi/\partial n|_{\partial\Omega} = 0$.

Since the quantity $\int_\Omega \phi(\mathbf{x},t)\,d\mathbf{x} = \int_\Omega \phi(\mathbf{x},0)\,d\mathbf{x} = \phi_0$ is conserved, without loss of generality we can consider that $\phi(\mathbf{x},t)$ possesses a vanishing initial mean, i.e., $\phi_0 = 0$. It follows from Eq. (1) that

$$\partial_t ||\phi||^2_{L^2}(t) = -2\varepsilon\,\frac{||\nabla\phi||^2_{L^2}(t)}{||\phi||^2_{L^2}(t)}\,||\phi||^2_{L^2}(t). \tag{3}$$

Therefore, the quantity $||\nabla\phi||^2_{L^2}(t)/||\phi||^2_{L^2}(t)$ is proportional (modulus a proportionality factor equal to $\varepsilon = \mathrm{Pe}^{-1}$) to the local decay rate of the norm of $\phi(\mathbf{x},t)$.

A. Mixing regimes: Early, intermediate, and asymptotic dynamics

The focus of this article is on the early-stage dynamics of an advecting-diffusing scalar field. A first basic issue to be properly framed is therefore the definition of what *early*, *intermediate*, and *asymptotic* mixing dynamics physically mean. The definition of these three mixing regimes should be unambiguous and based on the physical properties of the interplay between advection and diffusion.

First, consider a classical example, namely, the time-periodic sine flow [21] on the unit two-torus $\Omega = \mathcal{T}^2 = \{(x,y) \mid 0 \leqslant x,y \leqslant 1\}$, equipped with periodic boundary conditions at the end points. The velocity field is periodic in time and given by the expression

$$\mathbf{v}(\mathbf{x},t) = \begin{cases} \mathbf{v}_1(\mathbf{x}) = [\sin(2\pi y),0], & t \in [0,T_p/2) \\ \mathbf{v}_2(\mathbf{x}) = [0,\sin(2\pi x)], & t \in [T_p/2,T_p). \end{cases} \tag{4}$$

The parameter T_p represents the flow period. This simple flow system has been extensively studied since, by changing the flow period T_p, it is possible to modulate qualitatively

and quantitatively the chaotic character of the Lagrangian dynamics (metric and topological structure of the Poincaré section, value of the Lyapunov exponent and of the topological entropy, etc.) mimicking the properties of physically realizable mixing systems.

As for any advection-diffusion problem at a finite value of the Péclet number defined on a bounded closed domain or on a boundaryless manifold such as the two-dimensional torus in the presence of a smooth velocity field, the stroboscopic Floquet operator $P : L^2(\Omega) \to L^2(\Omega)$ associated with the advection-diffusion equation

$$P = e^{(-\mathbf{v}_2\cdot\nabla+\varepsilon\nabla^2)T_p/2} \circ e^{(-\mathbf{v}_1\cdot\nabla+\varepsilon\nabla^2)T_p/2} \tag{5}$$

is compact, and therefore it possesses a countable discrete spectrum of eigenvalues. Therefore, the asymptotic decay of any scalar field $\phi(\mathbf{x},t)$ solution of Eq. (1) for any $\varepsilon > 0$ is necessarily exponential, and for generic initial conditions (i.e., apart from a set of zero Lebesgue measure) it is controlled by the second eigenvalue ν_2 of the Floquet operator ($\nu_1 = 1$ by mass conservation, and the eigenvalues of P are ordered in a nonincreasing way with respect to their moduli). In a time-continuous frame, the dominant decay exponent is therefore given by $\Lambda(\mathrm{Pe}) = -\ln|\nu_2|/T_p$.

Figure 1 depicts the early and intermediate stages of the norm decay of ϕ, starting from a segregated initial condition $\phi_{t=0} = 1/\sqrt{2}$ for $0 \leqslant x < 1/2$, $\phi_{t=0} = -1/\sqrt{2}$ for $1/2 \leqslant x < 1$, at $\mathrm{Pe} = 10^4$ for several values of the flow period T_p. As can be observed, the intermediate scale dynamics seems to be characterized by an apparent power-law behavior of $||\phi||^2_{L^2}(t) \sim t^{-\kappa}$, which applies over one and half decades (curves b and c in Fig. 1) up to two and half decades (curve a in Fig. 1) depending on the flow period T_p. The values found for the apparent exponent κ are $\kappa = 3.3$ for $T_p = 0.56$, $\kappa = 1.6$ for $T_p = 1.18$, and $\kappa = 2.7$ for $T_p = 2$. There is no straightforward connection between the value of the intermediate-range apparent exponent κ and the geometric and dynamic properties of the Poincaré section of the flow kinematics. The case $T_p = 0.56$ possesses large islands of periodicity and the exponent κ is definitely higher than for

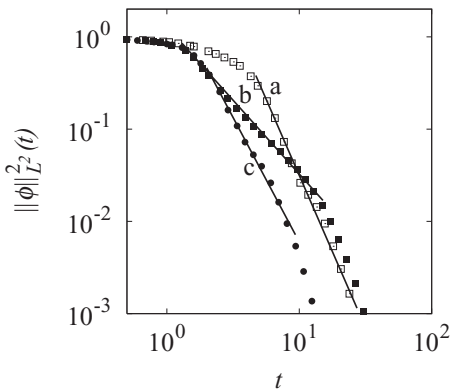

FIG. 1. Decay of $||\phi||^2_{L^2}(t)$ vs t for the time-periodic sine flow at $\mathrm{Pe} = 10^4$ and for different values of the flow period T_p. Line a and symbols (open square) $T_p = 0.56$, line b and symbols (filled square) $T_p = 1.18$, line c and symbols (closed circle) $T_p = 2$. The solid lines are the intermediate power-law fittings $||\phi||^2_{L^2}(t) \sim t^{-\kappa}$, with $\kappa = 3.3$ at $T_p = 0.56$, $\kappa = 1.6$ at $T_p = 1.18$, $\kappa = 2.7$ at $T_p = 2$.

$T_p = 1.18$ (the Poincaré section of which possesses much smaller islands), and larger than for $T_p = 2$ which is apparently globally chaotic in a measure-theoretical sense and possesses four parabolic fixed points.

In general, the evolution of an advecting-diffusing scalar field can be subdivided into three main stages (see Supplemental Material for a brief discussion of the mixing regimes [22]):

(i) An *early-stage regime* in which the interface separating fluid elements increases in a purely kinematic way (for scalar field possessing zero mean, this interface corresponds to the zero-level set $\Gamma_0(t) = \{[x_0(t), y_0(t)] \mid \phi[x_0(t), y_0(t), t] = 0\}$), and diffusion acts only transversally to this interface. This early-stage regime ends up when different fluid elements, separated by narrow striations, coalesce due to diffusion.

(ii) An *intermediate regime* in which a complex restructuring of the spatial profile occurs. This is due to the continuous formation of material interface triggered by convection and the subsequent smoothening and coalescence due to diffusion.

(iii) The *asymptotic regime* in which the function $||\nabla\phi||^2_{L^2}(t)/||\phi||^2_{L^2}(t)$ oscillates around a well defined mean value, proportional to the dominant decay exponent. In this regime, the spatial profile of the scalar field has a prevalent contribution from the dominant eigenfunction (for generic initial conditions), the decay of $||\phi||_{L^2}(t)$ is exponential in time and is controlled by the dominant decay exponent Λ.

From the above schematization, several relevant physical observations follow. First, the early stages and the asymptotic regimes admits a well-posed physical characterization, while the intermediate regime corresponds essentially to the mixing dynamics separating the early-stage evolution from the asymptotic behavior. It is not surprising that the intermediate-time properties in the scalar decay can be very difficult to derive from the properties of the advection-diffusion operator. The complexity of the intermediate-stage mixing results in the occurrence of a variety of different *apparent* intermediate scaling behaviors (see Fig. 1), and by the fact that these scaling behaviors strongly depend on the initial conditions.

Therefore, any attempt in analyzing the dynamics of a mixing process with a focus on the initial mixing stages, with the purpose of deriving closed-form expressions for the scalar decay, should necessarily rely on what was defined above as the early-stage dynamics. The analysis of Meunier and Villermaux [11], although focused on other features of the mixing process, addresses this early time scale.

B. Flow systems and prototypical model

In the previous paragraph, we have discussed the temporal structure of a mixing process in a closed system, outlining the relevance of the early-stage dynamics. In order to attempt a theoretical analysis of this regime, it is convenient to consider first some prototypical models amenable to a complete theoretical investigation, and only afterward to tackle the issue of generic Stokes flows. These models are reviewed in this section.

Consider the autonomous sine-flow system [21], namely, the autonomous flow on the two-torus $\mathcal{T}^2 = \{(x,y) \mid 0 \leqslant x < 1\,,\, 0 \leqslant y < 1\}$ in the presence of a sinusoidal velocity field $\mathbf{v} = [V_m \sin(2\pi y), 0]$. In nondimensional form, the

advection-diffusion equation for a scalar field ϕ reads as

$$\partial_t \phi = -\sin(2\pi y)\,\partial_x \phi + \frac{1}{\mathrm{Pe}}\left(\partial_x^2 \phi + \partial_y^2 \phi\right), \tag{6}$$

where $\mathrm{Pe} = V_m L/D$ is the Péclet number (L is characteristic length scale and D the diffusivity). Equation (6) is equipped with periodic boundary conditions on x and y, where $\mathrm{Pe} = V_m L/D$ is the Péclet number. Expanding the scalar field $\phi(x,y,t)$ in Fourier series with respect to x, i.e.,

$$\phi(x,y,t) = \sum_{m=-\infty}^{\infty} \phi_m(y,t)\, e^{i2\pi m x}, \tag{7}$$

the advection-diffusion equation decouples into a countable family of parabolic systems for the quantities $\phi_m(y,t)$, $m = \ldots, -1,0,1,\ldots$:

$$\partial_t \phi_m(y,t) = -i2\pi m\, \sin(2\pi y)\,\phi_m(y,t) + \frac{1}{\mathrm{Pe}}\,\partial_y^2 \phi_m(y,t) - \frac{4\pi^2 m^2}{\mathrm{Pe}}\,\phi_m(y,t), \tag{8}$$

which represent the Schrödinger-type non-Hermitian formulation of the advection-diffusion equation in the presence of an imaginary potential.

The imaginary potential formulation of the advection-diffusion equation derived for parallel flows on the torus applies also to simple channel flows. Consider a two-dimensional (2D) channel flow in the presence of a parallel velocity field $\mathbf{v} = [V_m v(y/W),0]$ in a channel of length L and width W, equipped with periodic boundary conditions at the end sections. By rescaling the coordinates $x/L \mapsto x \in (0,1)$, $y/W \mapsto y \in (0,1)$, $t \mapsto t V_m/L$, the nondimensional evolution equation for ϕ is identical to Eq. (6) with $\sin(2\pi y)$ replaced by $v(y)$, and with the Laplacian contribution along the axis x multiplied by the reciprocal of the square of the geometrical aspect ratio $\alpha = L/W \gg 1$. Consequently, the Péclet number is here defined as $\mathrm{Pe} = V_m W^2/DL$, and is the ratio of the characteristic diffusion time $t_{\mathrm{diff}} = W^2/D$ along the transverse direction, and the mean (convective) residence time $t_{\mathrm{adv}} = L/V_m$.

As periodic boundary conditions along x are assumed, the scalar field ϕ can be expanded in Fourier series (7), so that the equation for the Fourier components $\phi_m(y,t)$ becomes

$$\partial_t \phi_m(y,t) = -i2\pi m v(y)\,\phi_m(y,t) + \frac{1}{\mathrm{Pe}}\,\partial_y^2 \phi_m(y,t) - \frac{4\pi^2 m^2}{\alpha^2\,\mathrm{Pe}}\,\phi_m(y,t), \tag{9}$$

which is altogether similar to Eq. (8).

The two examples described above refer to closed bounded systems. However, the imaginary-potential formulation encompasses also the description of simple open systems operating at steady state, as well as channel flows operating in a time-pulsating way. These two cases are briefly outlined as follows.

Consider the flow between two coaxial cylinders of inner and outer radii R_{in} and R_{out}, respectively, where $R_{out} = R_{in} + r_\delta$, $r_\delta \ll R_{in}$, driven in the axial direction by a pressure drop and by the rotation of the inner and outer cylinders. This flow can be referred to as the Couette-Poiseuille flow, the velocity field of which admits nonvanishing angular and axial components. Under Stokes conditions, the velocity field is expressed in a cylindrical reference system by $\mathbf{v} = [0, v_\theta(r), v_z(r)]$, where r is the radial coordinate and z the axial one. If the length of the tube is much greater than the characteristic cross-sectional width $r_\delta = R_{out} - R_{in}$, the contribution of axial diffusion can be neglected with respect to transverse diffusion. This follows straightforwardly by the Taylor-Aris analysis of dispersion [23,24], and has been thoroughly discussed for cylindrical tubes in [25]. Due to periodicity on θ, the steady-state scalar field $\phi(r,\theta,z)$ can be expanded in Fourier series with respect to the angular variable θ, namely, $\phi(r,\theta,z) = \sum_{m=-\infty}^{\infty} \phi_m(r,z) e^{im\theta}$, thus reducing the advection-diffusion equation to an imaginary potential form for each of the Fourier coefficients $\phi_m(r,z)$, $m = \ldots, -1,0,1,\ldots$:

$$v_z(r)\,\partial_z \phi_m(r,z) = -\frac{i\,m\,v_\theta(r)}{r}\,\phi_m(r,z) + \frac{D}{r}\,\partial_r(r\,\partial_r \phi_m) - \frac{D\,m^2}{r^2}\,\phi_m(r,z). \tag{10}$$

If the spacing between the two cylinders is very small compared to the inner radius, i.e., $r_\delta/R_{in} \ll 1$, the advection-diffusion equation can be linearized by respect to the scaled cross-sectional coordinate $y = (r - R_{in})/r_\delta \in (0,1)$. In this way, Eq. (10) simplifies to a Cartesian nondimensional form, leading to the equation

$$w(y)\,\partial_\xi \phi(y,\xi) = \varepsilon\,\partial_y^2 \phi(y,\xi) + i\,V(y)\,\phi(y,\xi) - \varepsilon'\,\phi(\xi,y), \tag{11}$$

where $\xi = z/L$ and $\phi_m(y,\xi)$ has been replaced (for notational simplicity) by $\phi(y,\xi)$. In Eq. (11) the weight function $w(y)$ is proportional to the axial velocity v_z and the potential $V(y)$ to the angular velocity v_θ/r. This model has been discussed in [15,26], and for details the reader is referred to these articles. Observe in this case that the coordinate $\xi = z/L$ represents a nondimensional axial coordinate (since a steady-state mixing problem in an open-flow device is considered), and that the weight function $w(y)$ accounts for the axial velocity component. Therefore, under no-slip boundary conditions, $w(y)$ vanishes at the end points $y = 0,1$ (i.e., at the tube walls), meaning that $w^{-1}(y)$ is singular at $y = 0$ and 1. For the Cartesian Couette-Poiseuille flow, the nondimensional weight function equals $w(y) = 6y(1-y)$ (Poiseuille flow), while the potential $V(y)$, in the case of equal and opposite rotation of the inner and outer cylinders, is given by $V(y) = \kappa(-1+2y)$, where κ is proportional to the ratio of the transverse-to-axial velocities.

It is important to observe that the time evolution of closed and bounded mixing systems fulfilling Eqs. (8) or (9) can be viewed as a special case of Eq. (11). Indeed, the positions $\xi = t$, $w(y) = 1$, $\varepsilon = \mathrm{Pe}^{-1}$, $V(y) = -2\pi m \sin(2\pi y)$, $\varepsilon' = 4\pi^2 m^2/\mathrm{Pe}$ reduces Eq. (8) to the form (11). Therefore, Eq. (11) is a very flexible model structure: if ξ is interpreted as an axial coordinate, then Eq. (11) describes steady-state properties of simple static mixers. In this case, $w(y)$ represents the axial velocity profile. Conversely, if ξ is a time coordinate, Eq. (11) describes transient behavior in closed mixing system. In this case, $w(y) = 1$, identically.

Equation (11) represents the prototypical model for unveiling the early-stage [early-time or short-length, deepening on the physical meaning of Eq. (11), and of the variable ξ, as discussed above] mixing dynamics, starting from simple functional theoretical arguments. In Eq. (11), $y \in (0,1)$, $\xi > 0$, $\varepsilon > 0$, $\varepsilon' > 0$. Moreover, the real-valued functions $w(y)$ and $V(y)$ entering Eq. (11) are such that $w(y) \geqslant 0$, while $V(y)$ can attain both positive and/or negative values. Equation (11) is equipped with the homogeneous Neumann boundary conditions

$$\partial_y \phi|_{y=0,1} = 0. \tag{12}$$

The field ϕ is complex valued, and we assume an initial and inlet condition of the form

$$\phi|_{\xi=0} = \phi_{\text{in}} = \text{constant}. \tag{13}$$

While y in general corresponds to a coordinate transverse to the flow, the coordinate ξ can be viewed, depending on the flow system, either as a nondimensional time (for closed-flow systems) or as a nondimensional axial coordinate (for channel flows, operating at steady conditions). In the former case, $w(y) = 1$. In the latter case, the weight function $w(y)$ represents physically the axial velocity profile that depends on the transverse coordinate y, while the potential $V(y)$ accounts for the transverse velocity field. The parameter ε is the reciprocal of the Péclet number $\text{Pe} = t_{\text{diff}}/t_{\text{adv}}$, which is the ratio of the characteristic diffusion and advection times. The parameter ε', whenever present (see below), expresses the effects of molecular diffusion acting parallel to the flow direction. Since Eq. (11) describes a wealth of different physical flow conditions, it is referred to as the generalized one-dimensional imaginary potential formulation of an advection-diffusion problem for a scalar field ϕ.

There is another interesting operating condition associated with mixing and dispersion in channel flows leading to the imaginary potential formulation (11), corresponding to time-periodic pulsating inlet conditions of the chemical species to be mixed. In microfluidic literature, this operating condition is referred to as *time-interleaved sequential segmentation* [27,28]. For details, see [22].

To sum up, Eq. (11) is the prototypical system considered, describing the modal dynamics of the Fourier coefficients for a wealth of different simple but physically significant mixing systems.

C. Modulus-phase equations

Let us express $\phi(y,\xi)$ in terms of its modulus $R(y,\xi)$ and phase $\varphi(y,\xi)$ [29]:

$$\phi(y,\xi) = R(y,\xi)\, e^{i\varphi(y,\xi)}. \tag{14}$$

Multiplying Eq. (11) by the complex conjugate ϕ^*, and the complex conjugate of Eq. (11) by ϕ, and summing and subtracting the resulting equations, one obtains

$$w(y)(\phi^*\partial_\xi\phi + \phi\partial_\xi\phi^*) = \varepsilon\left(\phi^*\partial_y^2\phi + \phi\partial_y^2\phi^*\right) - 2\varepsilon'|\phi|^2, \tag{15}$$

$$w(y)(\phi^*\partial_\xi\phi - \phi\partial_\xi\phi^*) = \varepsilon\left(\phi^*\partial_y^2\phi - \phi\partial_y^2\phi^*\right) + 2iV(y)|\phi|^2. \tag{16}$$

Since

$$\phi^*\partial_\xi\phi + \phi\partial_\xi\phi^* = 2R\,\partial_\xi R, \tag{17}$$

$$\phi^*\partial_y^2\phi + \phi\partial_y^2\phi^* = 2R\,\partial_y^2 R - 2R^2(\partial_y\varphi)^2, \tag{18}$$

$$\phi^*\partial_\xi\phi - \phi\partial_\xi\phi^* = 2\,i\,R^2\,\partial_\xi\varphi, \tag{19}$$

$$\begin{aligned}\phi^*\partial_y^2\phi - \phi\partial_y^2\phi^* &= 4\,i\,R\,\partial_y R\partial_y\varphi + 2iR^2\partial_y^2\varphi \\ &= 2i\partial_y(R^2\partial_y\varphi),\end{aligned} \tag{20}$$

Eqs. (15) and (16) become

$$w(y)\,\partial_\xi R = \varepsilon\partial_y^2 R - \varepsilon(\partial_y\varphi)^2 R - \varepsilon' R, \tag{21}$$

$$w(y)\,R^2\,\partial_\xi\varphi = \varepsilon\partial_y(R^2\partial_y\varphi) + V(y)R^2, \tag{22}$$

which express the advection-diffusion equation in the modulus-phase formalism.

Multiplying Eq. (21) by R and Eq. (22) by φ and integrating over $y \in (0,1)$, the following energetic equalities can be obtained:

$$\begin{aligned}\frac{1}{2}\,\partial_\xi||R||_w^2(\xi) &= -\varepsilon||\partial_y R||_{L^2}^2(\xi) - \varepsilon||R\,\partial_y\varphi||_{L^2}^2(\xi) \\ &\quad - \varepsilon'||R||_{L^2}^2(\xi),\end{aligned} \tag{23}$$

$$\begin{aligned}\frac{1}{2}\int_0^1 w(y)\,R^2(y,\xi)\partial_\xi\varphi^2(y,\xi)\,dy \\ = -\varepsilon||R\,\partial_y\varphi||_{L^2}^2(\xi) + (V,R^2\,\varphi)(\xi),\end{aligned} \tag{24}$$

where

$$\begin{aligned}||R||_{L^2}^2(\xi) &= \int_0^1 R^2(y,\xi)\,dy, \\ ||R||_w^2(\xi) &= \int_0^1 w(y)\,R^2(y,\xi)\,dy, \\ ||\partial_y R||_{L^2}^2(\xi) &= \int_0^1 [\partial_y R(y,\xi)]^2 dy, \\ ||R\,\partial_y\varphi||_{L^2}^2(\xi) &= \int_0^1 R^2(y,\xi)\,[\partial_y\varphi(y,\xi)]^2 dy, \\ (V,R^2\,\varphi)(\xi) &= \int_0^1 V(y)\,R^2(y,\xi)\,\varphi(y,\xi)\,dy.\end{aligned} \tag{25}$$

In deriving Eqs. (23) and (24), the homogeneous Neumann boundary conditions (12) have been applied, leading for the modulus and phase to the analogous conditions $\partial_y R(y,\xi)|_{y=0,1} = 0$, $\partial\varphi(y,\xi)|_{y=0,1} = 0$.

III. SHORT-TIME BEHAVIOR OF THE IMAGINARY POTENTIAL MODEL AND UNIVERSALITY

This section is aimed exclusively at the analysis of the early-stage properties of Eq. (11) in order to show the occurrence of two different qualitative universal scalings depending on the regularity properties of the two functions $V(y)$, $w(y)$ entering Eq. (11). Following Giona *et al.* [16,17], the asymptotic spectral properties associated with Eq. (11), such as localization patterns, eigenvalue scaling, etc., are controlled by the effective potential

$$V_{\text{eff}}(y) = \frac{V(y)}{w(y)}. \tag{26}$$

As it will be discussed in this section, the short-term properties of the solutions of Eq. (11) also depend on the nature of $V_{\rm eff}(y)$.

Two distinct cases should be considered separately: (i) whether $V_{\rm eff}(y)$ is a smooth function of $y \in (0,1)$ or (ii) $V_{\rm eff}(y)$ diverges at some points in the interval $(0,1)$, including the boundary point $y = 0, 1$. The first case occurs for closed-flow models, for which ξ represents a nondimensional time and $w(y) = 1$, identically. The second case occurs for channel flows, by considering steady or pulsatile mixing patterns, whenever the axial velocity profile $w(y)$ admits some stagnation points. In no-slip flows, this occurs at the channel walls. We consider smooth, i.e., nonimpulsive initial conditions. The case of impulsive conditions is briefly outlined in Sec. IV.

As addressed in the following, the short-term behavior of the scalar field ϕ solution of Eq. (11) is "universal," meaning that its functional scaling with respect to the coordinate ξ does not depend on the fine structure of the two functions $w(y)$ and $V(y)$, but solely on the singularity versus regularity of the effective potential $V_{\rm eff}(y)$.

A. Nonsingular effective potentials

This section addresses the case of a smooth $V_{\rm eff}(y)$. In order to obtain an analytic expression for the early stages of the mixing process, it is necessary to make some approximations for the leading terms controlling the dynamics. In this perspective, the modulus-phase equations (21) and (22) provide the most convenient formal setting for simplifying the dynamics.

Consider Eqs. (21) and (22). For small ε, at the early stages, the phase dynamics is controlled by the term $V(y)R^2$, with $R \simeq 1$, since $V(y)R^2 \sim \mathcal{O}(1)$, while $\varepsilon\partial_y(R^2\partial_y\varphi) \sim \mathcal{O}(\varepsilon)$. Therefore, Eq. (22) at early stages simplifies as

$$\partial_\xi \varphi(y,\xi) = V_{\rm eff}(y), \tag{27}$$

i.e., the diffusive contribution in the phase dynamics can be neglected with respect to the forcing term associated with the action of the potential $V(y)$.

Similarly, in the modulus equation, the term $-\varepsilon(\partial_y\varphi)^2 R \sim \mathcal{O}(\varepsilon)$ is order of ε, while $\varepsilon\partial_y^2 R \sim \mathcal{O}(\varepsilon^2)$, as can be checked by elementary perturbation methods and *ex post* from the approximated solution so obtained (see below). This implies that the modulus evolution at the early stages can be described by the simplified equation

$$w(y)\,\partial_\xi R(y,\xi) = -\varepsilon\,(\partial_y\varphi)^2\,R(y,\xi) - \varepsilon' R(y,\xi), \tag{28}$$

meaning that the modulus dynamics is controlled by the gradient of the phase. Since $\varphi(y,0) = 0$, from Eq. (27) it readily follows that

$$\varphi(y,\xi) = V_{\rm eff}(y)\,\xi, \tag{29}$$

and Eq. (28) becomes

$$\partial_\xi R(y,\xi) = -\left[\frac{\varepsilon\,[V'_{\rm eff}(y)]2\,\xi^2}{w(y)} + \frac{\varepsilon'}{w(y)}\right] R(y,\xi), \tag{30}$$

where $V'_{\rm eff}(y) = dV_{\rm eff}(y)/dy$.

Observe that the solution (29) satisfies the condition (13), namely, $\varphi(y,\xi = 0) = 0$. Since $R(y,\xi = 0) = 1$, the modulus profile resulting from Eq. (30) is given by

$$R(y,\xi) = \exp\left[-\frac{\varepsilon[V'_{\rm eff}(y)]^2\,\xi^3}{3\,w(y)} - \frac{\varepsilon'\,\xi}{w(y)}\right]. \tag{31}$$

Observe from Eq. (31) that $\varepsilon\partial_y^2 R \sim \mathcal{O}(\varepsilon^2)$ since $\varepsilon' \sim \mathcal{O}(\varepsilon)$. A further quantitative numerical validation of these approximations can be found in [22].

The case $w(y) = 1$, as discussed in Sec. II, corresponds to the early-time dynamics of closed and bounded mixing systems, upon the identification of ξ with the time variable t. In this case, from Eq. (31), the L^2 norm of the scalar field ϕ decays at the early stages as

$$||\phi||_{L^2}(\xi) = \exp\left[-\varepsilon'\,\xi - \frac{\varepsilon}{3}[V'(\overline{y})]^2\,\xi^3\right], \tag{32}$$

where $\overline{y}$ is some internal point in the interval $(0,1)$, and $||\phi||_{L^2}(0) = 1$. Consequently,

$$-\ln||\phi||_{L^2}(\xi) = \varepsilon'\,\xi + \frac{\varepsilon\,[V'(\overline{y})]^2}{3}\,\xi^3. \tag{33}$$

Equation (33) predicts the following early-stage scaling:

$$-\ln||\phi||_{L^2}(\xi) \sim \begin{cases} \xi & \text{for } \xi < \xi_c, \\ \xi^3 & \text{for } \xi > \xi_c, \end{cases} \tag{34}$$

where the crossover abscissa ξ_c can be vanishing, whenever $\varepsilon' = 0$. Equation (34) is independent of the fine details characterizing the spatial profiles of $w(y)$ and $V(y)$, and consequently can be viewed as a universal scaling for this class of advection-diffusion problems.

Let us discuss several examples. Consider the Poiseuille flow $[w(y) = 1,\ V(y) = 6y(1-y),\ \varepsilon' = 0]$. In this case, at short times,

$$||\phi||^2_{L^2}(\xi) = \int_0^1 R^2(y,\xi)\,dy = \exp\left[-\frac{2\,\varepsilon}{3}[V'(\overline{y})]^2\,\xi^3\right]. \tag{35}$$

Therefore, the early-stage evolution for different values of $\mathrm{Pe} = \varepsilon^{-1}$ can be rescaled into a single master curve, for a given flow system, by considering the lumped variable $\overline{\xi} = \varepsilon^{1/3}\xi$. This invariant rescaling, which is a straightforward consequence of Eq. (35), is depicted in Fig. 2 in the case of the Poiseuille flow.

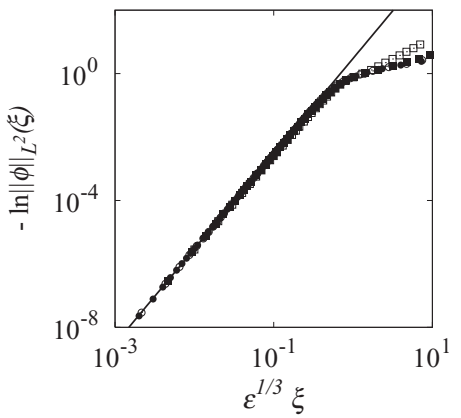

FIG. 2. Invariant rescaling of the initial norm: $-\ln||\phi||_{L^2}(\xi)$ vs $\varepsilon^{1/3}\xi$ for the 2D Poiseuille flow. Symbols (open square) refer to $\varepsilon = 10^{-3}$, (filled square) to $\varepsilon = 10^{-4}$, (open circle) to $\varepsilon = 10^{-5}$, (filled circle) to $\varepsilon = 10^{-6}$. The solid line represents the graph of the curve $-\ln||\phi||_{L^2}(\xi) = 3\,(\varepsilon^{1/3}\,\xi)^3$.

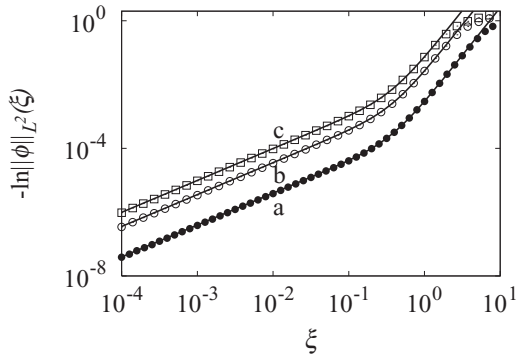

FIG. 3. $-\ln||\phi||_{L^2}(\xi)$ vs ξ for the modal evolution of the autonomous sine flow at $\varepsilon = 10^{-5}$ for different values of m. Symbols (filled circle) refer to $m = 1$, (open circle) to $m = 3$, (open square) to $m = 5$. The solid lines are the theoretical predictions based on Eq. (36).

The crossover behavior described by Eq. (34) occurs, e.g., in the autonomous sine flow, where $[V'(y)]^2 = 16\pi^4 m^2 \cos^2(2\pi y)$. The value of $\overline{y}$ can be chosen as the abscissa at which the function $\cos^2(2\pi y)$ attains its intermediate value $\frac{1}{2}$, in this way $[V'(\overline{y})]^2 = 8\pi^4 m^2$. The groups ε and ε' are related to the Péclet number by the equations $\varepsilon = 1/\mathrm{Pe}$, $\varepsilon' = 4\pi^2 m^2/\mathrm{Pe} = 4\pi^2 m^2 \varepsilon$, so that Eq. (33) specializes for the mth mode of the sine flow as

$$-\ln||\phi||_{L^2}(\xi) = 4\pi^2 m^2 \varepsilon\, \xi + \frac{8\pi^4 m^2 \varepsilon}{3}\, \xi^3. \qquad (36)$$

Figure 3 depicts the initial scaling of $-\ln||\phi||_{L^2}(\xi)$ in the sine flow at $\varepsilon = 10^{-5}$ for different values of the integer m, compared with the theoretical prediction (36). The simulations refer to an initial uniform concentration $\phi|_{\xi=0} = 1$. The agreement between theory and numerical simulations is excellent.

B. Singular effective potential

A completely different behavior characterizes the short-term properties of the solutions of Eq. (11) in the presence of a singular effective potential. The analysis developed in this paragraph is a more thorough elaboration of the scaling theory proposed in a paper [28] for time-pulsating channel flows, and applies on equal footing to generic open-flow systems for which $w(y)$ possesses some stagnation point. In point of fact, all the numerical examples supporting the theory refer to steady-state operations in channel flows and not to time-pulsating inlet conditions.

Since $V(y)$ is smooth in physically significant transport problems, the occurrence of singularities for $V_{\mathrm{eff}}(y)$ is associated with the zeros of $w(y)$. In channel flows, Eq. (11) describes the steady-state mixing behavior along the nondimensional axial coordinate ξ, and consequently $w(y)$ is a normalized nondimensional representation of the axial velocity profile. For no-slip flows, the singularities in $V_{\mathrm{eff}}(y)$ are thus localized at the channel walls $y = 0, 1$.

As a model system, consider the Cartesian Couette-Poiseuille flow described by Eq. (11) with $\varepsilon' = 0$, where $V(y) = -1 + 2y$ and $w(y) = 6y(1-y)$. Figure 4 shows the behavior of $1 - ||\phi||_{L^2}(\xi)$ for this flow system at several values of ε starting from a uniform inlet condition $\phi|_{\xi=0} = 1$, which

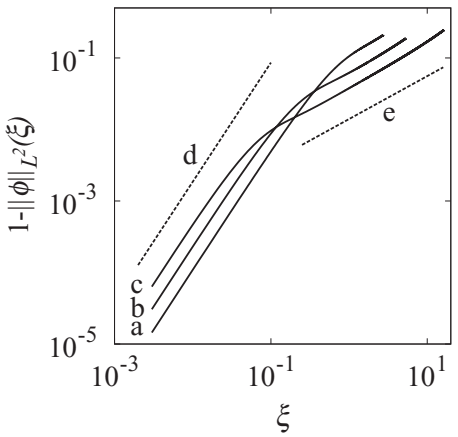

FIG. 4. $1 - ||\phi||_{L^2}(\xi)$ vs ξ for 2D channel flow (Cartesian Couette-Poiseuille flow) with $V(y) = -1 + 2y$, $w(y) = 6y(1-y)$ at different values of $\varepsilon = 10^{-3}$ (line a), 10^{-4} (line b), 10^{-5} (line c). Dashed lines d and e represent the scaling laws $1 - ||\phi||_{L^2}(\xi) \sim \xi^{5/3}$ and $1 - ||\phi||_{L^2}(\xi) \sim \xi^{3/5}$, respectively. The data have been obtained numerically using a truncated Galerkin expansion for the scalar field, as discussed in the main text.

implies $R|_{\xi=1} = 1$, $\varphi|_{\xi=1} = 0$. These data have been obtained numerically, expanding the concentration field in Fourier series $\phi(y,\xi) = \sum_{n=0}^{N} \phi_n(\xi)\cos(n\pi y)$, enforcing a very large number of Fourier coefficients, i.e., $N \simeq 10^5$, and integrating the resulting system of differential equations for $\{\phi_n(\xi)\}$, using a fourth-order Runge Kutta algorithm. A crossover behavior occurs between two qualitatively different regimes, leading to the scaling

$$1 - ||\phi||_{L^2}(\xi) = \begin{cases} \xi^{5/3}, & \xi < \xi_c \\ \xi^{3/5}, & \xi > \xi_c \end{cases} \qquad (37)$$

where ξ_c is the crossover abscissa (see Fig. 4). At the very early stages of the process, a $\frac{5}{3}$ power-law scaling is observed for the quantity $1 - ||\phi||_{L^2}(\xi)$, which successively shifts into a $\frac{3}{5}$ power-law behavior. This transition corresponds to two well-defined physical phenomenologies associated with the occurrence of two qualitatively different mixing regimes, the properties of which can be understood by considering the spatial behavior of the modulus $R(y,\xi)$ in the neighborhood of the singularity point $y = 0$ (a perfectly symmetric situation occurs at the other channel wall, located at $y = 1$).

Figure 5(a) depicts the very early stages of the process, corresponding to the formation of a thin depletion region [where the modulus $R(y,\xi)$ deviates from 1] close to the stagnation point $y = 0$ of the axial velocity profile. As ξ increases, the depletion proceeds progressively up to a situation at which the modulus $R(y,\xi)$ at $y = 0$ is practically vanishing. This very early stage of the mixing process can be referred to as the *depletion regime*, where a boundary layer close to $y = 0$ is formed (and by symmetry, an analogous boundary layer occurs at the symmetric wall $y = 1$). Once the depletion at $y = 0$ is completed, i.e., $R(0,\xi) = 0$, another mixing regime occurs, as depicted in Fig. 5(b), where the modulus for increasing ξ behaves as a moving front with dispersion traveling away from the stagnation point. This new regime can be referred to as the *traveling wave regime*.

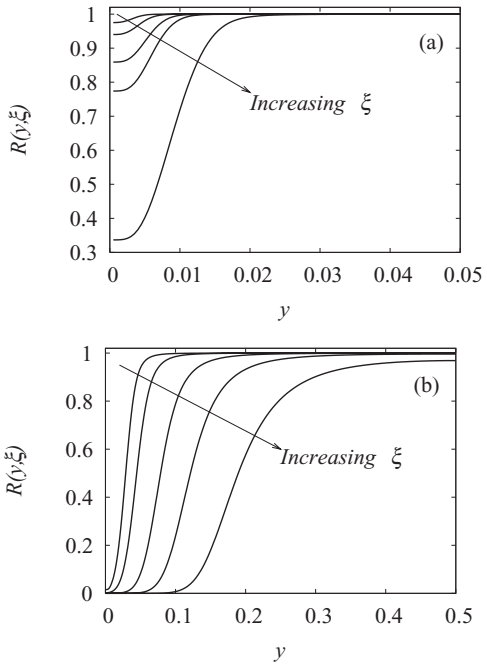

FIG. 5. $R(y,\xi)$ vs y for the model discussed in the main text $[V(y) = -1 + 2y,\ w(y) = 6y(1-y)]$ at $\varepsilon = 10^{-5}$ for different ξ (the arrows indicate increasing values of ξ). (a) Depletion regime, $\xi = 5\times10^{-3}, 10^{-2}, 2\times10^{-2}, 3\times10^{-2}, 10^{-1}$. (b) Traveling-wave regime, $\xi = 1, 2, 5, 10, 20$.

The physics of these two phenomena can be conveniently understood by enforcing the modulus-phase decomposition of the advection-diffusion equation. Before developing this analysis, it is convenient to observe that the two early-stage regimes (i.e., the depletion and the traveling wave regimes) originate from the formation and extension of a mixing boundary layer close to the stagnation point. Therefore, it is convenient to make use of classical boundary layer approximations, consisting in assuming the transverse coordinate unbounded [i.e., considering $y \in (0,\infty)$], and in linearizing the velocity profiles near $y = 0$. The first assumption is fully motivated by the fact that solely a small neighborhood close to $y = 0$ is influenced by the phenomenon, while for large y the modulus $R(y,\xi)$ remains at the uniform inlet value $R(y,0) = 1$. The second approximation implies that one can consider for the weight function $w(y)$ and for the potential $V(y)$ the leading order terms is a series expansion, namely,

$$w(y) = w_0\, y, \quad V(y) = V_0, \tag{38}$$

where $w_0 = dw(y)/dy|_{y=0} \neq 0$ and $V_0 = V(y=0) \neq 0$.

First, consider the depletion regime depicted in Fig. 5(a). In the depletion regime $R \simeq 1$, so that phase dynamics simplifies as

$$w_0\, y\, \partial_\xi \varphi = \varepsilon\, \partial_y^2 \varphi + V_0, \tag{39}$$

where the boundary layer linearizations (38) have been enforced. This equation is defined for $y \in (0,\infty)$, and it is equipped with the boundary conditions $\varphi|_{\xi=0} = 0$, $\varphi|_{y=0} = 0$. The solution of Eq. (39) can be sought in an invariant form

$$\varphi(y,\xi;\varepsilon) = \varepsilon^p\, \xi^\alpha\, y^\beta\, f(\xi\, \varepsilon^q\, y^{-\gamma}), \tag{40}$$

where the dependence of the phase on ε has been indicated, and $f(\eta)$ is a function of the lumped variable $\eta = \xi\, \varepsilon^q\, y^{-\gamma}$. Substituting the latter expression into the phase dynamics, Eq. (39) reduces to an ordinary differential equation for the rescaled variable η provided that the exponents entering Eq. (40) are given by

$$p = -\tfrac{1}{3}, \quad \alpha = \tfrac{2}{3}, \quad \beta = 0, \quad q = 1, \quad \gamma = 3. \tag{41}$$

Therefore, the invariant solution of Eq. (39) attains the functional form

$$\varphi(y,\xi;\varepsilon) = \varepsilon^{-1/3}\, \xi^{2/3}\, f(\xi\, \varepsilon\, y^{-3}). \tag{42}$$

From Eq. (42) it follows that $\partial_y \varphi = -3\, \varepsilon^{2/3} \xi^{5/3} y^{-4} f'(\xi \varepsilon y^{-3})$, where $f'(\eta) = df(\eta)/d\eta$, so that

$$\varepsilon\, (\partial_y \varphi)^2 = 9\, \varepsilon^{7/3}\, \xi^{10/3}\, y^{-8}\, [f'(\eta)]^2, \tag{43}$$

where $\eta = \xi \varepsilon y^{-3}$. Since $y^{-1} = (\eta \xi^{-1} \varepsilon^{-1})^{1/3}$, thus $y^{-8} = \eta^{8/3}\, \xi^{-8/3}\, \varepsilon^{-8/3}$, and therefore Eq. (43) can be rewritten as

$$\begin{aligned} \varepsilon\, (\partial_y \varphi)^2 &= 9\, \varepsilon^{-1/3}\, \xi^{2/3}\, \eta^{8/3}\, [f'(\eta)]^2 \\ &= \varepsilon^{-1/3}\, \xi^{2/3}\, h(\eta), \end{aligned} \tag{44}$$

where $h(\eta) = 9\, \eta^{8/3}\, [f'(\eta)]^2$. Substituting the latter expression for $\varepsilon(\partial_y \varphi)^2$ into the evolution equation (21) for $R(\xi, y; \varepsilon)$, one obtains

$$w_0\, y\, \partial_\xi R = \varepsilon\, \partial_y^2 R - \varepsilon^{-1/3}\, \xi^{2/3}\, h(\eta)\, R. \tag{45}$$

Since $R|_{\xi=0} = 1$, it is convenient to introduce the new variable $\rho(y,\xi;\varepsilon) = 1 - R(y,\xi;\varepsilon)$, so that $\rho|_{\xi=0} = 0$. The last term in Eq. (45) thus becomes $\varepsilon^{-1/3}\, \xi^{2/3}\, h(\eta)\, (1-\rho)$, and since ρ is very small at the short-term stages of the process, ρ can be neglected with respect to 1 in the factor $(1-\rho)$. As a consequence, Eq. (45) reduces to

$$w_0\, y\, \partial_\xi \rho = \varepsilon\, \partial_y^2 \rho + \varepsilon^{-1/3}\, \xi^{2/3}\, h(\eta). \tag{46}$$

Equation (46) too admits an invariant rescaled solution

$$\rho(y,\xi;\varepsilon) = \varepsilon^{-2/3}\, \xi^{4/3}\, g(\xi\, \varepsilon\, y^{-3}), \tag{47}$$

which can be obtained by applying the same approach adopted above for the phase function.

Starting from the invariant solution (47), an estimate for the norm decay can be obtained. In the depletion regime, $R(y,\xi)$ is very close to 1, apart from the depletion zone close to the stagnation point $y = 0$. Let $\delta(\xi)$ be the width of the mixing boundary layer, i.e., of the region close to $y = 0$ where $R(y,\xi)$ deviates from 1 [see Fig. 5(a)]. The difference $1 - ||\phi||_{L^2}(\xi)$ is approximately equal to the area of the triangle possessing base equal to $\delta(\xi)$ and height $1 - R(0,\xi)$, where $R(0,\xi)$ is the value of the modulus at $y = 0$ [see Fig. 5(a)]. Therefore,

$$1 - ||\phi||_{L^2}(\xi) = \tfrac{1}{2}\, [1 - R(0,\xi)]\, \delta(\xi) = \tfrac{1}{2}\, \rho(\xi,0)\, \delta(\xi). \tag{48}$$

It follows from Eq. (47) that

$$\rho(0,\xi) = \varepsilon^{-2/3}\, \xi^{4/3}\, g_\infty, \tag{49}$$

where $g_\infty = \lim_{\eta\to\infty} g(\eta)$. For the width $\delta(\xi)$ of the mixing boundary layer one can assume an expression of the form

$$\delta(\xi) = \frac{\int_0^\infty y |\partial_y R(y,\xi)|\, dy}{\int_0^\infty |\partial_y R(y,\xi)|\, dy}. \tag{50}$$

In point of fact, the specific choice of the definition (50) for the width of the mixing boundary layer is immaterial, in the meaning that alternative, physically consistent, expressions for $\delta(\xi)$ would produce the same scaling for the norm decay as a function of ξ.

Substituting the invariant rescaled expression for $1 - R(y,\xi)$ into Eq. (50), after some manipulations, it results that

$$\delta(\xi) \sim \varepsilon\, \xi^{1/3}. \tag{51}$$

Consequently, from Eqs. (49) and (51), it follows that

$$1 - ||\phi||_{L^2}(\xi) \sim \varepsilon^{-1/3}\, \xi^{5/3}. \tag{52}$$

Equation (52) explains the very early-stage $\frac{5}{3}$ scaling found for singular potentials and depicted in Fig. 4.

Let us now analyze the traveling-wave regime. As discussed in [28], the traveling-wave regime is controlled by the phase singularity occurring at the stagnation point. This implies that the contributions $\varepsilon(\partial_y\varphi)^2$ and $V(y)\,R^2$ in the modulus and phase dynamics [Eqs. (21) and (22)] are predominant with respect to the remaining diffusive contributions. Therefore, phase dynamics simplifies as

$$\partial_\xi \varphi = \frac{V_0}{w_0\, y}, \tag{53}$$

i.e.,

$$\varphi(\xi,y) = \frac{V_0\, \xi}{w_0\, y}, \tag{54}$$

and the modulus dynamics (21) becomes

$$\partial_\xi R = -\frac{\varepsilon}{w_0\, y}\,(\partial_y\varphi)^2\, R = -\frac{\varepsilon\, V_0^2\, \xi^2}{w_0\, y^5}\, R. \tag{55}$$

Equation (55) can be solved starting with the inlet condition $R(0,y) = 1$ to give

$$R(y,\xi) = \exp\left[-\frac{\varepsilon\, V_0^2\, \xi^3}{3\, w_0\, y^5}\right]. \tag{56}$$

Observe that $R(y,\xi)$ vanishes identically at $y = 0$ for $\xi > 0$ in the traveling-wave regime.

As can be observed from the graph of $R(y,\xi)$ depicted in Fig. 5(b), the difference $1 - ||\phi||_{L^2}(\xi)$ in the traveling-wave regime is substantially equal to the width of the mixing boundary layer $\delta(\xi)$:

$$1 - ||\phi||_{L^2}(\xi) \simeq \delta(\xi). \tag{57}$$

From Eqs. (56) and (57) it follows after some simple algebraic manipulations (not reported here for the sake of brevity) that

$$\delta(\xi) = \int_0^\infty y\,\partial_y R(y,\xi)\, dy \sim \xi^{3/5}, \tag{58}$$

as observed numerically in Fig. 4. This result completes the analysis of the early-stage dynamics in the presence of singular effective potentials.

IV. GLOBAL SHORT-TERM PROPERTIES

In Sec. III, we have outlined the short-term universal features exhibited by Eq. (11) in the presence of an imaginary potential. In this section, we explore how the the universal scaling laws obtained in Sec. III for the modal components should be composed and weighted with respect to the initial concentration distribution to obtain global short-term properties by considering the autonomous sine-flow equation (6) as a prototype.

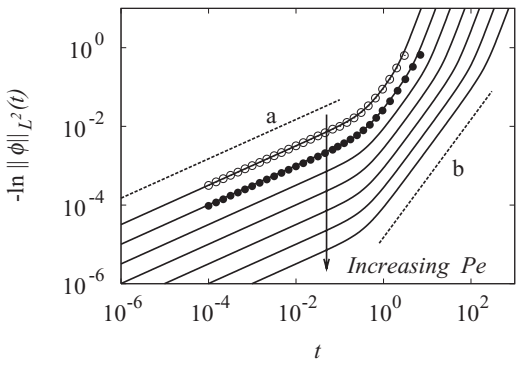

FIG. 6. $-\ln||\phi||_{L^2}(t)$ vs t obtained by applying Eq. (63) for the sine flow at different Péclet numbers. The arrow indicates increasing values of Pe $= 10^4, 10^5, 10^6, 10^7, 10^8, 10^9, 10^{10}$. Dashed line (a) represents the scaling $-\ln||\phi||_{L^2}(t) \sim t^{1/2}$, dashed line (b) $-\ln||\phi||_{L^2}(t) \sim t^{3/2}$. Symbols [(open circle) Pe $= 10^4$, (filled circle) Pe $= 10^5$] refer to the numerical simulation of Eq. (6).

Consider Eq. (6) and let us assume a segregated initial profile

$$\phi(x,y,t)|_{t=0} = \begin{cases} -1 & \text{for } x < 1/2, \\ 1 & \text{for } x > 1/2. \end{cases} \tag{59}$$

Figure 6 [symbols (open circle) and (filled circle)] depicts the initial norm decay of the scalar field ϕ for two different values of the Péclet number. As can be observed, the very early dynamics follows a stretched exponential behavior

$$||\phi||_{L^2}(t) \simeq \exp(-c\sqrt{t}), \tag{60}$$

where c is a time-independent parameter that depends on Pe. Equation (60) implies that the logarithm of the L^2 norm of ϕ with reversed sign is proportional to the square root of time (dashed line a in Fig. 6). The numerical data depicted in Fig. 6 have been obtained by expanding the concentration field in a truncated Fourier series $\phi(x,y,t) = \sum_{m,n=_N}^{N} \phi_{m,n}(t) e^{i2\pi(mx+ny)}$ by considering a very large number of Fourier modes ($N = 30\,000$). Such an accurate and computationally expensive numerical simulation is necessary in order to reproduce correctly the initial concentration decay since the initial condition $\phi_{m,n}(0)$ associated with Eq. (59) is a slow decaying function of m:

$$\phi_{m,n}(0) = i\,\frac{(1-\delta_{m,0})\,\delta_{n,0}}{\pi\, m}\,[1-(-1)^m]. \tag{61}$$

The result expressed by Eq. (60) finds a straightforward explanation by enforcing the universal scaling behavior analyzed in Sec. III. From Eq. (36), by expanding ϕ in Fourier modes with respect to x, $\phi(x,y,t) = \sum_{m=-\infty}^{\infty} \phi_m(y,t)\, e^{i2\pi mx}$, it follows that the norm decay of each mode is given by

$$||\phi_m||_{L^2}(t) = |\phi_m(0)|\, \exp(-4\pi^2 m^2 \varepsilon\, t - 8\pi^4 m^2 \varepsilon t^3/3). \tag{62}$$

Since $|\phi_m(0)| = 2/(\pi m)$ for m odd and zero otherwise, the early-stage decay of the L^2 norm of ϕ is given by

$$||\phi||_{L^2}(t) = \left[\sum_{m=1}^{\infty} \frac{8}{\pi^2(2m-1)^2} \exp[-8\pi^2(2m-1)^2\varepsilon\, t - 16\pi^4(2m-1)^2\varepsilon t^3/3]\right]^{1/2}. \quad (63)$$

Observe that the summation in Eq. (63) is extended to positive odd integers weighted twice, as negative values of m contribute with the same factor as positive integers. The solid lines in Fig. 6 represent the function (63). For very short times, the linear term in the argument of the exponentials entering Eq. (63) prevails with respect to the cubic contribution ($\sim t^3$). Therefore,

$$||\phi||_{L^2}(t) \simeq \sqrt{B(t,q)|_{q=8\pi^2\varepsilon}}, \quad (64)$$

where the function $B(t,q)$ is given by

$$B(t,q) = \sum_{m=1}^{\infty} \frac{8}{\pi^2(2m-1)^2} \exp[-q(2m-1)^2 t]. \quad (65)$$

The scaling of the function $B(t,q)$ with respect to time t can be obtained by replacing the summation with an integral

$$\begin{aligned} B(t,q) &\sim \int_1^{\infty} e^{-qtx^2} \frac{dx}{x^2} \\ &= e^{-qt} - \sqrt{\pi q t}[1 - \mathrm{erf}(\sqrt{qt})] \\ &= G(q\,t) \end{aligned} \quad (66)$$

[the result expressed by Eq. (66) is reported in [30]], where $\mathrm{erf}(x) = (2/\sqrt{\pi}) \int_0^x e^{-y^2} dy$ is the error function. For $q\,t < 10^{-2}$ the function $G(q\,t)$ can be accurately approximated as

$$G(q\,t) \simeq e^{-\sqrt{\pi\, q\, t}}. \quad (67)$$

Equation (67) explains the observed scaling equation (60) at the very early times. The result obtained above can be extended to longer time scales. Specifically, Fig. 6 depicts the behavior of $||\phi||_{L^2}(t)$ obtained from Eq. (63) for very high Péclet values (up to $\mathrm{Pe} = 10^{10}$). As the Péclet number increases, it becomes more evident the crossover from the early $-\ln||\phi||_{L^2}(t) \sim t^{1/2}$ scaling to the subsequent $-\ln||\phi||_{L^2}(t) \sim t^{3/2}$ decay. In point of fact, this crossover is also evident from the numerical simulation of the advection-diffusion equation (symbols) depicted in Fig. 6. Also, this phenomenon can be easily interpreted from what was discussed above. At later times, the cubic contribution in the argument of the exponential entering Eq. (63) becomes predominant with respect to the linear term. Therefore, the decay of the L^2 norm of ϕ is essentially given by

$$\begin{aligned} &||\phi||_{L^2}(t) \\ &= \left[\sum_{m=1}^{\infty} \frac{8}{\pi^2(2m-1)^2} \exp[-16\pi^4(2m-1)^2\varepsilon t^3/3]\right]^{1/2} \\ &\simeq \sqrt{B(t^3,q)|_{q=16\pi^4\varepsilon/3}}, \end{aligned} \quad (68)$$

and from the scaling relation (67) it follows that

$$||\phi||_{L^2}(t) \sim \exp(-c\, t^{3/2}), \quad (69)$$

where c is a positive parameter independent of time, as observed numerically. This example is indicative of the fact that starting from the scaling predicted for the class of model systems [Eq. (11)], it is possible to explain and predict the early-stage behavior of more complex flows. This issue is further addressed in the next section by considering physically realizable model systems.

It is useful to discuss further the physical meaning and the implications of the early-stage solutions (60) and (69) obtained from segregated (and initially discontinuous) profiles. In point of fact, Eq. (60) holds for purely diffusive transport [31]. As the Péclet number increases (i.e., for $\varepsilon \to 0$), the effective practical relevance of the early diffusive decay is practically immaterial, and the $e^{-ct^{3/2}}$ behavior (69) controls, *de facto*, the initial dynamics. This decay regime is indeed a consequence of the interplay between transverse diffusion and the action of the flow field. Therefore, Eq. (69) can be properly viewed as a *convection-controlled* initial decay. We return to this issue in the next section. The analysis developed for the initial profile (59) can be extended to generic initial profiles by summing the contribution of each of the Fourier modes weighted with respect to the initial conditions $|\phi_m(0)|^2$. In all the cases in which $|\phi_m(0)|^2 \sim 1/m^2$, one expects from scaling arguments to observe generically the global norm decay scaling expressed by the stretched exponential function $\exp(-b_1 t^{1/2} - b_2 t^{3/2})$, where the contribution of the very early diffusive behavior becomes progressively less significant as Pe increases.

Different initial scalings occur in the presence of impulsive initial conditions. To give an example, consider the impulsive initial profile,

$$\phi(x,y,t)|_{t=0} = \delta(x - x_c) - 1 \quad (70)$$

localized along a line, where x_c is a generic abscissa in $(0,1)$. This initial profile is not square summable, and its Fourier coefficients are in modulus equal to $|\phi_m(0)| = 1$ for $m \neq 0$ and $|\phi_0(0)| = 0$. Therefore, the early stage decay can be expressed as

$$||\phi||_{L^2}(t) = \left[2\sum_{m=1}^{\infty} \exp(-8\pi^2 m^2 \varepsilon\, t - 16\pi^4 m^2 \varepsilon t^3/3)\right]^{1/2}. \quad (71)$$

Using the same approach applied for segregated initial profiles (see [22]), one obtains at very early stages

$$||\phi||_{L^2}(t) \sim \left(\frac{Pe}{t}\right)^{1/4}. \quad (72)$$

Figure 7 shows the comparison of the theoretical predictions based on Eqs. (71) and (72) with the numerical results for the autonomous sine flow at two different values of Pe, confirming the early-stage $\frac{1}{4}$ scaling. At later times, an intermediate scaling $||\phi||_{L^2}(t) \sim t^{-3/4}$ sets in as a consequence of the cubic terms in the argument of the exponentials entering Eq. (71). This phenomenon becomes more pronounced as the Péclet number increases.

There is one further case that can be considered to complete the picture, namely, that of an impulsive initial condition localized at some point (x_c, y_c):

$$\phi(x,y,t)|_{t=0} = \delta(x - x_c)\delta(y - y_c) - 1. \quad (73)$$

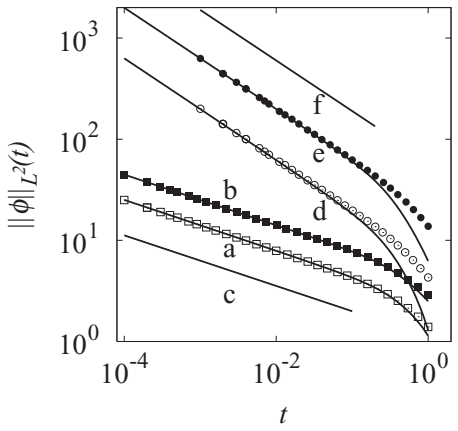

FIG. 7. $||\phi||_{L^2}(t)$ vs t for the autonomous sine flow in the presence of the impulsive initial conditions (70) and (73). Symbols (open square) refer to $\mathrm{Pe} = 10^3$, (filled square) to $\mathrm{Pe} = 10^4$ for (70). Lines a and b represent Eq. (71) for the corresponding values of the Péclet number. Line c represents the scaling $||\phi||_{L^2}(t) \sim t^{-1/4}$. Symbols (open circle) refer to $\mathrm{Pe} = 10^3$, (filled circle) to $\mathrm{Pe} = 10^4$ for (73). Lines d and e represent Eq. (74) for the corresponding values of the Péclet number. Line f represents the scaling $||\phi||_{L^2}(t) \sim t^{-1/2}$.

This situation is interesting, as it implies an impulsive initial condition for the Fourier modes $\phi_m(y,t=0)$. Therefore, the theory developed in Sec. III does not apply straightforwardly. However, if one expands the concentration profile in a double Fourier series $\phi(x,y,t) = \sum_{m,n=-\infty}^{\infty} \phi_{m,n}(t)\, e^{2\pi i(mx+ny)}$, and enforces the analysis discussed above for the inlet condition (70), one can easily recognize that the very early mixing stages are controlled by pure diffusion and therefore $|\phi_{m,n}(t)| = e^{-4\pi^2 m^2 \varepsilon t}\, e^{-4\pi^2 n^2 \varepsilon t}$. By summing over all the modes, it follows that

$$||\phi||_{L^2}(t) \simeq 2B_\delta(t,q)|_{q=8\pi^2\varepsilon} \sim \left(\frac{Pe}{t}\right)^{1/2}, \qquad (74)$$

where $B_\delta(t,q) = \sum_{q=1}^{\infty} e^{-qm^2 t}$ (see also [22]). Equation (74) predicts an initial power-law decay with an exponent equal to $\frac{1}{2}$, i.e., twice as large than in the case of a lineal impulsive condition (70). Figure 7 shows the results of numerical simulations, confirming the theoretical prediction. For high Péclet values, this initial decay is followed by an intermediate power-law scaling $||\phi||_{L^2}(t) \sim t^{-3/2}$, which is a consequence of the interplay between diffusion and advection. We return to this issue in Sec. VI.

V. SHORT-TERM DECAY IN AUTONOMOUS STOKES FLOWS

In the previous section, we have used an autonomous flow on the two-torus (the sine flow) to show how the information deriving from the short-time decay of single Fourier modes can be composed and used to predict the variance decay associated to several different initial conditions. The sine-flow model is just a useful toy model, but it would be unrealistic to extrapolate from its behavior general results valid for autonomous Stokes flows unless a careful analysis is performed on more realistic flow models. This section considers physically realizable and model flows of increasing fluid-dynamic and kinematic complexity.

Specifically, we show that the results derived from the analysis developed in Sec. IV hold true even for physically realizable two-dimensional steady Stokes flows in wall-bounded domains, and even for autonomous partially chaotic flows. This section presents the result of numerical simulations. A theoretical explanation of them is addressed in Sec. VI.

A. Two-dimensional Stokes flows

There are simple physically realizable flows for which the theory developed in Secs. III and IV applies straightforwardly. This is the case of the Couette flow in the annular region between coaxial cylinders, a case that is strictly described by Eq. (11) in that the flow is unidirectional along a cyclic coordinate. The description of advection-diffusion dynamics in the Couette flow by means of a family of one-dimensional Schrödinger-type equation in the presence of an imaginary potential has been thoroughly developed in [18].

However, there are situations in which the reduction to Eq. (11) is by no means trivial. A typical example of this case is the Stokes flow within a square cavity with a sliding wall moving at constant unit velocity (lid-driven cavity flow). In principle, one can use an action-angle transformation [32] by enforcing the analogy between the stream function and the Hamiltonian function to recast the advection-diffusion equation in a form of non-Hermitian Schrödinger-type equation. We leave this analysis to future investigation and focus below on numerical simulations.

The advection-diffusion equation in the lid-driven cavity has been solved by expanding the concentration field in Fourier series $\phi(x,y,t) = \sum_{m,n=0}^{N} \phi_{m,n}(t)\cos(m\pi x)\cos(n\pi y)$ and solving the resulting linear system of differential equations for the Fourier coefficients $\phi_{m,n}(t)$.

Figure 8(a) shows the behavior of $-\ln||\phi||_{L^2}(t)$ for the lid-driven cavity flow in the case of a segregated nonimpulsive inlet condition $\phi_0 = 1$ for $x < \frac{1}{2}$, $\phi_0 = -1$ for $x > \frac{1}{2}$, at at three different values of the Péclet number: $\mathrm{Pe} = 10^3; 10^4; 10^5$. Aside from the initial dependence of $-\ln||\phi||_{L^2}(t)$ proportional to $t^{1/2}$, the regime $-\ln||\phi||(t) \sim t^{3/2}$ becomes more and more evident as the Pe values increase. This regime eventually breaks down to leave place to a smooth transition to the asymptotic exponential decay. The comparison of the mixing patterns at different times along the process [Figs. 8(b), 8(c), and 8(d)] with the decay regimes of Fig. 8(a) shows the different mixing mechanisms that are relevant in each regime. The initial square root decay exponent is essentially associated with the superposition of purely diffusive modes expressing the initial condition. The $\frac{3}{2}$ exponent instead arises as the consequence of the superposition of convection-enhanced decay exponents, as already observed for the sine-flow protocol. Note that in the lifespan of this regime, no significant interaction between neighboring lamellae as yet occurred [see Fig. 8(c)]. When the $\frac{3}{2}$ regime breaks down, the interaction between parallel lamellae becomes significant [Fig. 8(d)], and the scalar variance becomes almost entirely localized at the system walls. An interesting feature arising from the numerical simulations is that the breakdown of the $\frac{3}{2}$ regime occurs at the same value of scalar variance, independently of the Pe value.

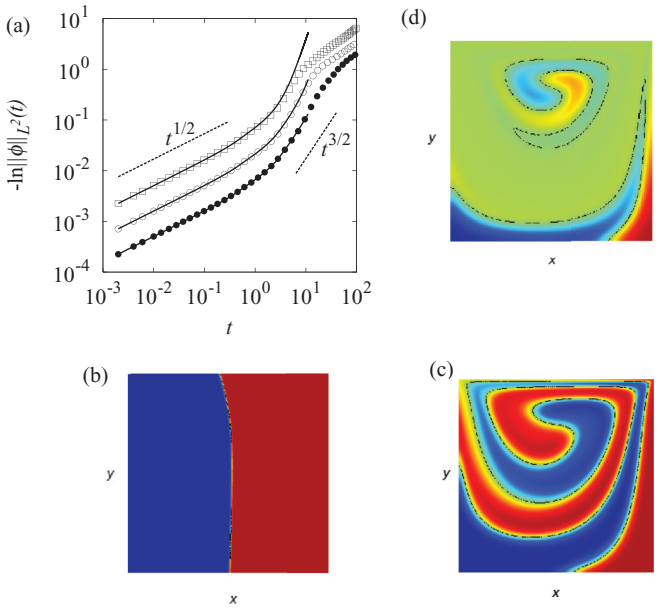

FIG. 8. (Color online) Short and intermediate variance decay regimes in the Stokes flow within a square cavity loaded with a step initial condition. (a) $-\ln||\phi||_{L^2}(t)$ vs t (open square): $\mathrm{Pe}=10^3$, (open circle): $\mathrm{Pe}=10^4$, (filled circle): $\mathrm{Pe}=10^5$. The solid lines are the kinematic predictions based on Eq. (83) and on the scaling of $\sigma(t)$. (b), (c), (d) Mixing patterns at $t=0.1$, $t=7.5$, $t=25$ at $\mathrm{Pe}=10^4$, respectively, corresponding to the different scaling regimes [compare with (a)].

By taking the lid-driven cavity flow as a prototypical example of a physically realizable system, it is possible to show the validity of the scaling results provided in Sec. IV also in the presence of impulsive initial conditions. Consider a localized inlet condition, namely, $\phi(\mathbf{x},t)|_{t=0}=\delta(\mathbf{x}-\mathbf{x}_c)-1$. Figure 9 depicts the initial dynamics of the norm of a scalar field and for two different choices of $\mathbf{x}_c$, namely, $\mathbf{x}_c=(0.5,0.5)$ and $\mathbf{x}_c=(0.1,0.1)$, i.e., very near the stagnation region close to the bottom wall, at several Péclet values. As expected from the theory developed in Sec. IV for impulsive initial conditions, the norm decay fulfills an initial $\frac{1}{2}$ power-law decay (independently of

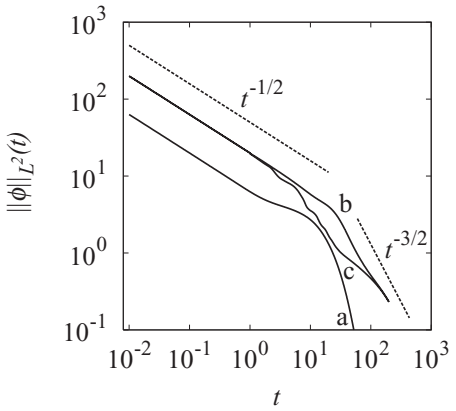

FIG. 9. $||\phi||^2_L(t)$ vs t for the lid-driven cavity flow in the presence of a localized initial condition centered at (x_c,y_c) Line a refers to $x_c=y_c=0.1$ at $\mathrm{Pe}=10^3$, line b to $x_c=y_c=0.1$ at $\mathrm{Pe}=10^4$, line c to $x_c=y_c=0.5$ at $\mathrm{Pe}=10^4$.

$\mathbf{x}_c$), followed by an intermediate $\frac{3}{2}$ power-law decay. This numerical result confirms the theoretical analysis developed in Sec. IV, and indicates that the scaling results developed in Sec. IV provide a rationale for predicting the early-stage decay of the norm of scalar field for generic autonomous flows in the presence of arbitrary initial conditions.

B. Three-dimensional chaotic flows

The model flows considered until now were two dimensional. In autonomous two-dimensional (incompressible) flows, the kinematics of passive particle is nonchaotic, as an integral of motion exists, represented by the stream function. In point of fact, the validity of the early-stage scaling discussed in Sec. IV, and confirmed above for 2D flows, seems to be a generic feature of autonomous systems and, consequently, there is no apparent reason why it should not hold also for three-dimensional flows, independently of their regular or chaotic nature. To support this claim, consider a classical model of autonomous chaotic flow, namely, the ABC [33] defined on the unit three-dimensional torus. This is a Beltrami flow [34], the velocity field $\mathbf{v}=(v_x,v_y,v_z)$ of which is given by

$$\begin{aligned} v_x &= A\,\sin(2\pi z)+C\,\cos(2\pi y),\\ v_y &= B\,\sin(2\pi x)+A\,\cos(2\pi z),\\ v_z &= C\,\sin(2\pi y)+B\,\cos(2\pi x). \end{aligned} \tag{75}$$

For $A=1/2\pi$, $B=\sqrt{2/3}/2\pi$, $C=\sqrt{1/3}/2\pi$, the kinematics of passive particle is partially chaotic [33].

Let us consider the advection-diffusion equation

$$\begin{aligned} \partial_t\phi = &-(v_x\,\partial_x\phi+v_y\,\partial_y\phi+v_z\,\partial_z\phi)\\ &+\varepsilon\left(\partial_x^2\phi+\partial_y^2\phi+\partial_z^2\phi\right), \end{aligned} \tag{76}$$

where (v_x,v_y,v_z) is given by Eq. (75), $\varepsilon=\mathrm{Pe}^{-1}$, and equipped with periodic boundary conditions at $x,y,z=0,1$. As an initial condition, consider the segregated zero-mean distribution

$$\phi|_{t=0}=\begin{cases}-1 & \text{for } x<1/2,\\ 1 & \text{for } x>1/2.\end{cases} \tag{77}$$

Figure 10 depicts the L^2 norm of $\phi(t,\mathbf{x})$ solution of Eqs. (76) and (77) at three different values of the Péclet number.

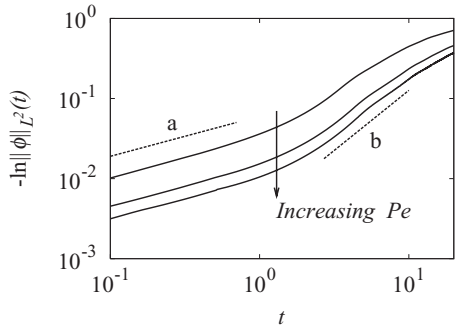

FIG. 10. $-\ln||\phi||_{L^2}(t)$ vs t for the 3D ABC flow equations (75) and (76), starting from the initial condition (77). The arrow indicates increasing values of $\mathrm{Pe}=10^4,\,5\times10^4,\,10^5$. Dashed line a represents the scaling $-\ln||\phi||_{L^2}(t)\sim t^{1/2}$, dashed line b the scaling $-\ln||\phi||_{L^2}(t)\sim t^{3/2}$.

The numerical simulations are performed by expanding the scalar field in a truncated Fourier series $\phi(t,\mathbf{x}) = \sum_{m,n,p=-N}^{N} \phi_{m,n,p}(t)\, e^{i2\pi(mx+ny+pz)}$, and integrating the resulting first-order system of ordinary differential equation for the Fourier coefficients $\phi_{m,n,p}(t)$. In order to reproduce accurately the initial decay, the value of N has been chosen equal to 120, corresponding to about 1.4×10^7 modes. As can be observed, the qualitative behavior of the short-time decay is altogether qualitatively identical to the decay observed in the sine flow and in the other two-dimensional flows considered in this section, displaying a crossover between a very early diffusive scaling $-\ln||\phi||(t) \sim t^{1/2}$ and a subsequent convection-driven stretched exponential behavior $-\ln||\phi||(t) \sim t^{3/2}$, corresponding to dashed lines a and b in Fig. 10, respectively.

VI. KINEMATIC ANALYSIS

As discussed in Sec. II, the early-stage dynamics is amenable to a kinematic description for generic autonomous flow systems. Specifically, the results obtained in the previous section for autonomous flows can be derived from a kinematic-based analysis of the early-stage dynamics by enforcing the warped-time transformation [11,35,36].

At the early stages, advection stretches the material interface (corresponding to the zero-level set of the ϕ for concentration fields possessing vanishing mean), and diffusion smoothens field gradients mainly in the direction transverse to the interface. As there is no merging between neighboring lamellae, these two processes can be easily accounted for. The approach followed is conceptually similar to the analysis developed in [11]. Let us consider an initial interface Γ_0 [in the case of segregated initial conditions (59) it corresponds to the straight vertical line at $x = \frac{1}{2}$], and let x and y be the local coordinates transversal and parallel to the interface. At the early stages, as discussed in [11], the diffusive contribution along the interface (i.e., in the x direction) can be neglected so that the advection-diffusion equation simplifies as

$$\partial_t \phi = -v_x\, \partial_x \phi - v_y\, \partial_y \phi + \varepsilon\, \partial_y^2 \phi. \tag{78}$$

At the early stages of the process, the interface experiences a stretching along y and a contraction along the transversal x direction. Let $L(t)$ be the length of the interface at time t, and $L(t=0) = L_0$. The local velocity field controlling the stretching and contraction processes can be expressed as [11,35,36]

$$v_x = \frac{x}{\sigma(t)} \frac{d\sigma(t)}{dt}, \quad v_y = -\frac{y}{\sigma(t)} \frac{d\sigma(t)}{dt}, \tag{79}$$

where $\sigma(t) = L(t)/L_0$. The magnitude of the ratio of the convective terms $v_y \partial_y \phi$, $v_x \partial_x \phi$ is proportional to the interface aspect ratio [11], and therefore $v_x \partial_x \phi$ can be neglected with respect to $v_y \partial_y \phi$ at the early mixing stages. This implies that Eq. (78) becomes

$$\partial_t \phi - \frac{y}{\sigma(t)} \frac{d\sigma(t)}{dt}\, \partial_y \phi = \varepsilon\, \partial_y^2 \phi. \tag{80}$$

Let us introduce the kinematically rescaled coordinates

$$\eta = y\, \sigma(t), \quad \tau = \varepsilon \int_0^t \sigma^2(t')\, dt' = \varepsilon \Sigma(t). \tag{81}$$

The variable τ is referred to as the *warped time* since it encompasses the stretching effects induced by the convective field. Since

$$\partial_t \phi = y \frac{d\sigma}{dt}\, \partial_\eta \phi + \varepsilon\, \sigma^2\, \partial_\tau \phi, \quad \partial_y \phi = \sigma\, \partial_\eta \phi, \quad \partial_y^2 \phi = \sigma^2\, \partial_\eta^2 \phi,$$

Eq. (81) becomes

$$y \frac{d\sigma}{dt}\, \partial_\eta \phi + \varepsilon\, \sigma^2\, \partial_\tau \phi - y \frac{d\sigma}{dt}\, \partial_\eta \phi = \varepsilon\, \sigma^2\, \partial_\eta^2 \phi,$$

and, after simplifications, it reduces to a purely diffusion equation in the rescaled coordinates:

$$\partial_\tau \phi = \partial_\eta^2 \phi. \tag{82}$$

Let g_D be the solution of Eq. (82) with the prescribed initial and boundary conditions, and $||g_D||_{L^2}(\tau)$ its L^2 norm. It follows from the definition of the warped time that

$$||\phi||_{L^2}(t) \simeq ||g_D||_{L^2}(\tau)|_{\tau = \varepsilon \int_0^t \sigma^2(t')\, dt'}. \tag{83}$$

For autonomous flows, $\sigma(t)$ grows at small t linearly with t, i.e.,

$$\sigma(t) \simeq \sqrt{1 + b\, t^2}, \tag{84}$$

where a is a constant depending on the velocity field. Therefore,

$$\tau \simeq \varepsilon \left(t + \frac{a\, t^3}{3} \right), \tag{85}$$

i.e., the warped time τ displays a crossover between the very early linear behavior proportional to t, and the later power-law scaling $\tau \sim t^3$. This kinematic analysis explains the scaling observed for generic Stokes flows, and is the Lagrangian counterpart of the functional analysis developed in Sec. IV. Moreover, it is also quantitatively predictive once the time evolution of $\sigma(t)$ is estimated for a given flow and a given initial condition. Let us discuss this observation in the light of all the examples analyzed in the previous section.

Consider first the case of the autonomous sine flow. For the segregated initial condition (59),

$$\sigma(t) = \int_0^1 \sqrt{1 + 4\pi^2 t^2\, \cos^2(2\pi y)}\, dy. \tag{86}$$

In this case, the solution of the diffusion equation provides $||g_D||_{L^2}^2(\tau) = \sum_{k=1}^{\infty} [8/\pi^2(2k-1)^2] \exp[-8\pi^2(2k-1)^2\, \tau]$. Figure 11(a) shows the comparison of the kinematic predictions based on Eq. (83) and of the numerical results for two values of Pe. The agreement is excellent.

In a similar way, the power-law scaling observed starting from impulsive conditions can be predicted analytically. In this case, g_D is the solution of the diffusion equation in the presence of an impulsive initial condition. At the very early stages, the norm of $g_D(\tau)$ can be approximated by that deriving from the solution of the diffusion equation in an infinite medium, i.e.,

$$||g_D||_{L^2}(\tau) \simeq \frac{1}{(8\pi\, \varepsilon\, \tau)^{1/2}}. \tag{87}$$

As it regards $\sigma(t)$ associated with the initial condition (73), consider a small circle of radius ρ centered at (x_c, y_c). At time t, the coordinates of its points advected by the sine-flow

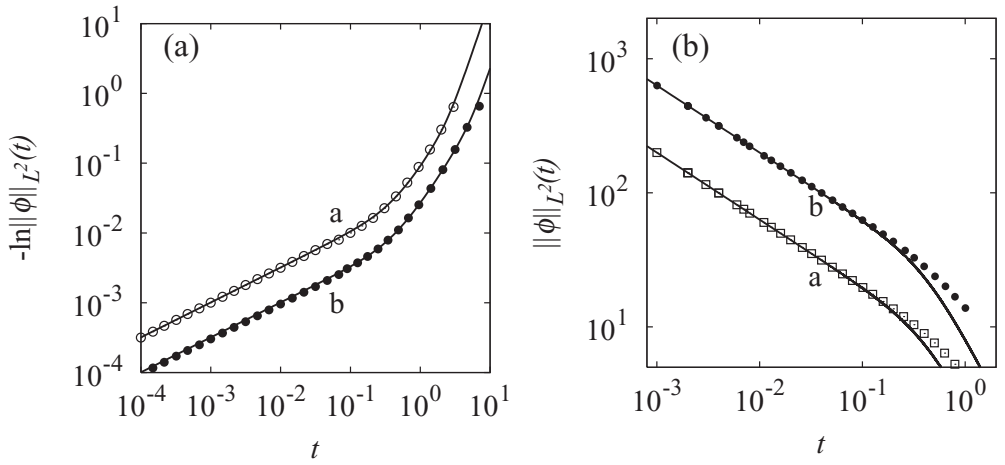

FIG. 11. Kinematic prediction based on Eq. (83) (solid lines) of the initial norm decay for the autonomous sine flow. (a) Segregated initial conditions. Line a and (open circle) refer to Pe $= 10^4$, line b and (filled circle) to Pe $= 10^5$. (b) Refers to an impulsive initial condition at $x_c = y_c = 0.5$. Line a and (open square) refer to Pe $= 10^3$, line b and (filled circle) to Pe $= 10^4$.

protocol are given by

$$x(\phi,t) = x_c + \rho\,\cos\phi + t\,\sin[2\pi(y_c + \rho\,\sin\phi)],$$
$$y(\phi,t) = y_c + \rho\,\sin\phi, \quad \phi \in [0,2\pi). \tag{88}$$

Therefore, $\sigma(t)$ can be expressed as

$$\sigma(t) = \lim_{\rho\to 0}\frac{1}{2\pi\rho}\int_0^{2\pi}\sqrt{\left(\frac{dx}{d\phi}\right)^2 + \left(\frac{dx}{d\phi}\right)^2}\,d\phi. \tag{89}$$

It can be observed from Eqs. (87)–(89) that the kinematic analysis predicts the transition from a power-law scaling $||\phi||_{L^2}(t) \sim t^{-1/2}$ to $||\phi||_{L^2}(t) \sim t^{-3/2}$ as observed numerically. Figure 11(b) shows the quantitative comparison of the kinematic approximation versus numerical simulations for impulsive initial conditions.

The comparison between kinematic predictions (solid lines) and numerical simulations for the cavity flow is depicted in Fig. 8(a) for segregated initial conditions. As the cavity is a closed domain equipped with homogeneous Neumann boundary conditions, the solution g_D of the diffusion equation in the rescaled coordinate should account for it. Consequently, the norm $||g||_{L^2}(\tau)$ is given by

$$||g_D||^2_{L^2}(\tau) = \sum_{k=1}^{\infty}\frac{8}{\pi(2k-1)^2}\exp[-2\pi^2(2k-1)^2\tau]. \tag{90}$$

VII. CONCLUDING REMARKS

This article has developed a first systematic analysis of the short-term properties of autonomous mixing systems by considering the class of model flows described by the Schrödinger-type equation (11) in the presence of an imaginary potential $iV(y)$ and of a non-negative weight function $w(y)$. As discussed in Sec. II, this prototypical system describes a wealth of different physical conditions, ranging from closed to open flows, from steady to unsteady and pulsating inlet conditions. The results found for this class of systems, once the dynamics of all of the Fourier modes is added together, are generic of the behavior observed in autonomous Stokes flows as shown numerically in Sec. IV and justified kinematically in Sec. V.

Essentially, the short-term properties associated with (11) are controlled by the singularity of the effective potential $V(y)/w(y)$, and universal short-term scaling laws have been derived from smooth and singular $V_{\rm eff}(y)$. It is important to stress that the concept of universality refers strictly to the class of transport problems described by Eq. (11) in that the stretched exponential versus power-law initial scaling does not depend on the fine details of the two functions $V(y)$ and $w(y)$ entering Eq. (11) but exclusively on the occurrence of singularities for $V(y)/w(y)$.

The kinematic approach developed in Sec. VI is the "Lagrangian" [as the scaling is controlled by the quantity $\sigma(t)$] counterpart of the functional analysis developed in Secs. III and IV. This approach is physically intuitive and fully predictive at early stages for generic initial conditions, as the function g_D and the behavior of $\sigma(t)$ depend on the mixing domain and on the initial concentration profile.

In discussing the qualitative properties of the mixing regimes and their time scales, we have analyzed in passing several model systems (time-periodic sine flow, two-dimensional lid-driven cavity flow), the early decay of which follows the theory presented in this paper. However, for longer time scale (intermediate mixing regime), an apparent power law is observed similarly to what was found in [13]. A thorough characterization of the intermediate-scale decay goes beyond the scope of this paper and will be developed elsewhere. Nevertheless, the results presented in Secs. II and IV and V provide some hints in the understanding of intermediate-scale mixing properties and can be summarized as follows: (i) a power-law behavior in $||\phi||^2_{L^2}(t)$ observed over more than two or three decades in the variance has no direct connection with the presence of solid no-slip boundaries in the mixing domain, as the case of the time-periodic sine flow shows; (ii) short-term power-law scalings are a consequence of impulsive initial conditions, corresponding to the localized injection of a dye tracer; (iii) the occurrence of these power-law scalings is an

intermediate-time manifestation of the rather complex modal decay in the relaxation towards the dominant eigenmode. Asymptotically, the scalar decay would follow eventually an exponential decay. This is ensured by the compactness of the Floquet operator (or of the stroboscopic operator) associated with the advection-diffusion equation. The analysis of intermediate-scale properties and the merging of the present, early-stage, theory with the asymptotic spectral theory, in order to achieve a global prediction of the decay of a scalar field, will be developed elsewhere.

[1] D. G. Baird and D. I. Collias, *Polymer Processing Principles and Design* (Wiley, New York, 1998).

[2] J. Kukura, P. C. Arratia, and E. S. Szalai, Pharmtech **26**, 48 (2002); M. M. Alvarez, J. M. Zalc, T. Shinbrot, P. E. Arratia, and F. J. Muzzio, AIChE J. **48**, 2135 (2002).

[3] N.-T. Nguyen and Z. Wu, J. Micromech. Microeng. **15**, R1 (2005).

[4] T. M. Squires and S. R. Quake., Rev. Mod. Phys. **77**, 977 (2005).

[5] A. Lasota and M. C. Mackey, *Chaos, Fractals, and Noise: Stochastic Aspects of Dynamics* (Springer, Berlin, 1998).

[6] S. Chandrasekhar, Rev. Mod. Phys. **15**, 1 (1943).

[7] N. S. Goel and N. Richter-Dyn, *Stochastic Models in Biology* (Academic, New York, 1974).

[8] A. N. Shiryaev, *Essentials of Stochastic Finance* (World Scientific, Singapore, 1999).

[9] V. I. Klyatskin, *Stochastic Equations through the Eye of the Physicist* (Elsevier, Amsterdam, 2005).

[10] S. Cerbelli, V. Vitacolonna, A. Adrover, and M. Giona, Chem. Eng. Sci. **59**, 2125 (2004).

[11] P. Meunier and E. Villermaux, J. Fluid Mech. **476**, 213 (2003).

[12] P. J. S. A. Ferreira de Sousa and J. C. F. Pereira, J. Fluid Mech. **634**, 41 (2009).

[13] E. Gouillart, N. Kuncio, O. Dauchot, B. Dubrulle, S. Roux, and J.-L. Thiffeault, Phys. Rev. Lett. **99**, 114501 (2007); E. Gouillart, O. Dauchot, B. Dubrulle, S. Roux, and J.-L. Thiffeault, Phys. Rev. E **78**, 026211 (2008).

[14] J.-L. Thiffault, E. Gouillart, and O. Dauchot, Phys. Rev. E **84**, 036313 (2011).

[15] J. P. Gleeson, O. M. Roche, J. West, and A. Gelb, SIAM J. Appl. Math. **64**, 1294 (2004); J. P. Gleeson, Phys. Fluids **17**, 100614 (2005).

[16] M. Giona, S. Cerbelli, and F. Garofalo, Europhys. Lett. **83**, 34001 (2008).

[17] M. Giona, S. Cerbelli, and V. Vitacolonna, J. Fluid Mech. **513**, 221 (2004).

[18] M. Giona, S. Cerbelli, and F. Garofalo, J. Fluid Mech. **639**, 291 (2009).

[19] S. Cerbelli, A. Adrover, F. Garofalo, and M. Giona, Microfluid. Nanofluid. **6**, 747 (2009).

[20] M. Giona and S. Cerbelli, Phys. Rev. E **81**, 046309 (2010).

[21] M. Liu, F. J. Muzzio, and R. L. Peskin, Chaos, Solitons Fractals **4**, 869 (1994); M. Giona, A. Adrover, S. Cerbelli, and V. Vitacolonna, Phys. Rev. Lett. **92**, 114101 (2004).

[22] See Supplemental Material at http://link.aps.org/supplemental/10.1103/PhysRevE.87.063011 for a brief discussion of the mixing regimes, for a detailed description of the mixing systems considered, and for further details on the leading terms controlling early-stage dynamics in the case of nonsingular effective potentials.

[23] G. Taylor, Proc. R. Soc. A **219**, 186 (1953).

[24] R. Aris, Proc. R. Soc. A **235**, 67 (1956).

[25] M. Giona, A. Adrover, S. Cerbelli, and F. Garofalo, Phys. Fluids **21**, 123601 (2009).

[26] M. Giona and S. Cerbelli, Phys. Rev. E **78**, 046303 (2008).

[27] J. T. Coleman and D. Sinton, Microfluid. Nanofluid. **1**, 319 (2005); Y. Huiqian, N.-T. Nguyen, and X. Huang X., J. Phys. Conf. Ser. **34**, 136 (2006); N.-T. Nguyen and X. Huang, Microfluid. Nanofluid. **1**, 373 (2005); Lab Chip **5**, 1320 (2005).

[28] F. Garofalo and M. Giona, Europhys. Lett. **93**, 54003 (2011).

[29] D. Bohm, Phys. Rev. **85**, 166 (1952).

[30] I. S. Gradshteyn and I. M. Ryzhik, *Table of Integrals, Series, and Products* (Academic, San Diego, 1980).

[31] J. Crank, *The Mathematics of Diffusion* (Clarendon, Oxford, 1975).

[32] H. Shin and M. R. Maxey, Phys. Rev. E **56**, 5431 (1997); D. L. Vainchtein, J. Widloski, and R. O. Grigoriev, *ibid.* **78**, 026302 (2008).

[33] T. Dombre, U. Frisch, J. M. Greene, M. Henon, A. Mehr, and A. M. Soward, J. Fluid Mech. **167**, 353 (1986); J. H. E. Cartwright, M. Feingold, and O. Piro, *ibid.* **316**, 259 (1996).

[34] D. D. Holm and Y. Kimura, Phys. Fluids A **3**, 1033 (1991).

[35] W. E. Ranz, AIChE J. **25**, 41 (1979).

[36] J. M. Ottino, *The Kinematics of Mixing: Stretching, Chaos and Transport* (Cambridge University Press, Cambridge, 1989).